Low Complexity Methods for Joint Detection and Synchronization of TDMA Bursts

Haotian Zhai and Bernd-Peter Paris
Department of Electrical and Computer Engineering
George Mason University
Fairfax, VA 22030
{hzhai,pparis}@gmu.edu

Abstract—This paper proposes a data-aided joint detection and synchronization algorithm for TDMA bursts. A sequential detection algorithm based on the Generalized Likelihood Ratio Test (GLRT) is used to detect the embedded preamble signal in received data stream. Carrier synchronization is attempted for each sample instant during sequential detection and resulting phase and frequency estimates are used by the GLRT. To make this algorithm implemented in software-defined radio (SDR), a low complexity carrier estimation algorithm with good estimation accuracy is proposed. Then, a refinement of the carrier estimate is computed when the preamble has been detected. It is shown that this estimate approaches the Cramer-Rao bound even at low SNR. The complete joint detection and estimation procedure is validated through simulations and SDR.

Index Terms—Joint detection and estimation, GLRT, low computational complexity, Cramer-Rao vector bound, Software-defined radio.

I. Introduction

In digital communication systems, information is commonly transmitted in time-multiplexed bursts. Examples include time-slotted random access systems. Each active user transmits information to the receiver in the same frequency band and in non-overlapping time intervals [1]. A fundamental prerequisite for successful coherent demodulation is that the receiver can detect the beginning of the data stream and estimate accurately the phase and frequency offset of the carrier. It is worth emphasizing that time and carrier synchronization are coupled problems: coherent methods for detecting the signal require accurate frequency and phase estimates while data-aided frequency and phase estimation requires that the location of the training sequence is available. Thus, joint signal detection and carrier synchronization algorithms play a vital role in any communication system; both accuracy and computational complexity of the algorithms must be considered.

Clearly, the signal acquisition problem has been considered widely. Many carrier estimation algorithms have been proposed for burst-mode transmission of digital data in the last 30 years. In the late 90's, Morelli and Mengali [2] presented a tutorial review of the field comparing such characteristics as estimation accuracy, range, and computational complexity of available techniques. The work by [3]–[8] is most closely related to results in this paper. For signal detection and time synchronization, algorithms have been developed for radar and radio systems with burst-mode transmission [9]–[14]. In these

works, the detection problem in the presence of unknown parameters (e.g., delay or Doppler shift) is usually solved by a Generalized Likelihood Ratio Test (GLRT).

Modern communication systems differ from those considered when the majority of synchronization algorithms were developed at least two key aspects. It is common now that communication systems operate at low SNR levels near 0 dB. At low SNR, it is critical to address detection and carrier acquisition jointly as non-coherent detection, assumed by the work cited in [2], is unreliable. Also, greatly increased data rates require that any synchronization algorithm is computationally efficient. Signal acquisition is the first step in the receiver's processing chain and must be performed in real time at the sample rate.

With these considerations in mind, this paper seeks to make the following contributions:

- We propose a low-complexity joint carrier estimation and detection algorithm; the per-sample computational complexity is linear in the length of the reference sequence.
- We offer new closed-form expressions for the distribution of the frequency estimate in the proposed algorithm; these are believed to be useful beyond this paper.
- The complete acquisition chain, including time and carrier synchronization, is analylzed and implemented in software-defined radio (SDR).

This paper first specifies our assumptions about the signal model. Then, the first step of the signal acquisition in this paper, i.e., the time synchronzation problem is addressed. Our algorithm is a sequential GLRT that relies on a joint frequency and phase estimate to facilitate coherent detection. Next, the focus shifts to estimating the carrier's phase and frequency offset. A family of low-complexity and high-accuracy estimation algorithms is proposed. Performance analysis of the complete system is provided through simulation. At the end of the paper, we perform the complete signal acquisition chain and the proposed joint detection and estimation algorithms on software-defined radio (SDR).

II. Signal Model

The transmitted signal burst is assumed to include a reference signal that is known to the receiver. Often such a reference sequence is prepended to the payload and is referred to as a preamble. The problem addressed in this paper is to accurately
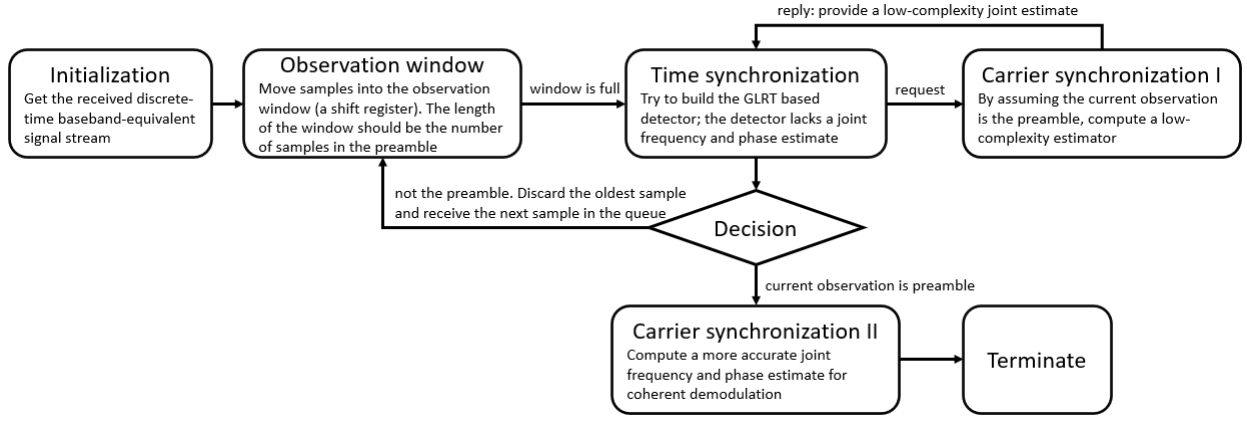
Fig. 1. Block diagram for analysis of the complete signal acquistion chain

estimate the start time of the preamble and to estimate carrier phase and frequency offset from this preamble. Hence, the payload portion of the burst is not further considered.

The baseband-equivalent reference signal $s(t)$ is digitally modulated as

$$s(t) = \sum_{i=0}^{L_0-1} c_i g(t - iT),\qquad(1)$$

where T denotes the symbol period and $g(t)$ provides pulse shaping. c_i are the known symbol sequence between transmitter and receiver, and L_0 is the number of symbols. It is common to assume the symbols $\{c_i\}$ have good autocorrelation properties to render coherent processing effective.

The received baseband equivalent signal stream are given by

$$r(t) = s(t - \tau) \cdot A e^{j\phi} e^{j2\pi f_d t} + w(t).\qquad(2)$$

where τ denotes the delay (the start time) of received reference signal in stream. A, ϕ, f_d are the carrier amplitude, phase, and frequency offset, respectively. These are the parameters to be estimated for signal acquisition. The complex, additive white Gaussian noise is denoted $w(t)$.

Our algorithms operate in discrete-time; sampling the received signal $r(t)$ at a rate of M samples per symbol, i.e., the sampling frequency $f_s = \frac{1}{T_s} = \frac{M}{T}$, yields

$$r_n = s_{n-p} A e^{j\phi} e^{j2\pi\delta n} + w_n,\qquad(3)$$

The continuous-time delay τ is decomposed into $\tau = pT_s + \Delta p$ with pTs integer multiples of sample period and the fractional delay Δp satisfying $-Ts/2 < \Delta p \leq T_s/2$. Δp is neglected in this paper because our proposed algorithm proceeds at a very sufficient sample rate (in SDR). $\delta = f_d T_s$ is the normalized frequency offset. Besides that, we use E_s/N_0 to represent the ratio of signal energy to noise power spectral density (SNR). Specifically, E_s is the averaged symbol energy of the received signal over the length of the preamble.

Our goal of this paper is to analyze the complete signal acquisition chain, which includes the detection (time synchronization) and joint phase and frequency estimation of the preamble (carrier synchronization). The procedure is depicted in Figure 1. The analysis of the signal acquisition chain will basically follow the steps that are shown in the figure as well as be implemented in software-defined radio (SDR).

III. DETECTION AND TIME SYNCHRONIZATION

As illustrated in Figure 1, the first step to analyze the signal acquisition chain is to formulate the detector. The algorithm proceeds sequentially and each step a window of length N (the number of samples in the preamble) received samples with $N-1$ overlapped samples is considered. The sequential detection problem solved in this paper is fundamentally equivalent to sequential frame synchronization [15]–[17].

The detection algorithm is based on a Generalized Likelihood Ratio Test (GLRT): Let H_0 be the null hypothesis that the preamble is not completely in the obeservation window against the alternative H_1 that it does. We further define Δ to be the distance between the current sample instant p_c and the true position of preamble p, i.e., $\Delta = p - p_c$. Thus, we can translate H_0 as when $\Delta \neq 0$ while H_1 as when $\Delta = 0$. The likelihood ratio test between H_0 and H_1 is given by

$$\Lambda(R) = \frac{p_{R|H_1}(r|H_1)}{p_{R|H_0}(r|H_0)} = \frac{\prod_{n=0}^{N-1} \frac{1}{\sqrt{\pi N_0}} \exp(-\frac{1}{2}\frac{|r_n - s_n S b^n|^2}{N_0/2})}{\prod_{n=\Delta}^{N-1} \frac{1}{\sqrt{\pi N_0}} \exp(-\frac{1}{2}\frac{|r_n - s_{n-\Delta} S b^n|^2}{N_0/2})} \cdot$$

$$\frac{1}{\prod_{n=0}^{\Delta-1} \frac{1}{\sqrt{\pi N_0}} \exp(-\frac{1}{2}\frac{|r_n|^2}{N_0/2})} \underset{H_0}{\overset{H_1}{\gtrless}} \eta,$$

$$\qquad(4)$$

where we define $S = A e^{j\phi}$, $b = e^{j2\pi\delta}$ for notation simplicity. Cancelling the common parts and taking the logarithm, (4) is reduced to

$$\Re\left\{\sum_{n=0}^{N-1} r_n s_n^* S^* b^{-n} - \sum_{n=\Delta}^{N-1} r_n s_{n-\Delta}^* S^* b^{-n}\right\} \underset{H_0}{\overset{H_1}{\gtrless}} \frac{N_0}{2}\ln\eta + \frac{A^2}{2}\sum_{n=N-\Delta}^{N-1}|s_n|^2. \tag{5}$$

The minuend of left hand side of (5) points to the inner product of the overlap between the observed (partial) preamble and the true preamble. By plugging r_n of hypothesis H_1, i.e., $r_n = s_n S b^n + w_n$, the minuend simplified as

$$\sigma(\Delta) = A^2 \sum_{n=\Delta}^{N-1} s_n s_{n-\Delta}^* + \sum_{n=\Delta}^{N-1} w_n s_{n-\Delta}^* S^* b^{-n} \tag{6}$$

is a Gaussian random variable with mean as a "partial" auto-correlation function (ACF) of the preamble at lag Δ. In order to quantify (6), the symbol sequence of the preamble should be chosen with a good autocorrelation property, such as Gold sequence, that the partial ACF is approximately equal to zero for all $\Delta \neq 0$. Thus, after some proper scaling of (5), the GLRT finally reduces to a function with respect to the current time instant p,

$$\frac{\Re\{\langle r_p, \hat{s}\rangle\}}{||r_p|| \cdot ||\hat{s}||} \underset{H_0}{\overset{H_1}{\gtrless}} \gamma \tag{7}$$

where $\hat{s}$ denote the carrier-estimate corrected reference samples, i.e., $\hat{s}_n = s_n A e^{j(2\pi\hat{\delta}n + \hat{\phi})}$ for $n = 0, \ldots, N-1$. r_p are the current observed received samples. Thus, we can intepret (7) as the generalized correlation between current observed burst and carrier-estimates corrected reference sequence. γ is the detection threshold which lies on the range of $[0, 1]$.

We see that building the GLRT detector of (7) relies on the frequency and phase estimates (carrier synchronization) first. Furthermore, since the sequential detection proceeds at every time instant, to make it work in practice, the complexity of the carrier estimates becomes much crucial. A low computational-complexity estimator should be derived for detection purpose.

IV. FREQUENCY AND PHASE ESTIMATION

Frequency and phase estimation (carrier synchronization) is the next step after detection for coherent demodulation. In this section, we discuss the estimation algorithm by assuming the time synchronization of the preamble is perfect, i.e., the current observation window contains the complete preamble.

For estimating frequency offset δ and the phasor $S = Ae^{j\phi}$, the maximum likelihood (ML) estimate of (3) is given by

$$\hat{\delta}, \hat{S} = \min_{\delta, S=Ae^{j\phi}} \sum_{n=0}^{N-1} |r_n - s_n S e^{j2\pi\delta n}|^2. \tag{8}$$

By taking the Wirtinger derivative with respect to S and setting it equal to zero, a closed form for the estimated phasor $\hat{S}$ is readily derived,

$$\hat{S} = \frac{\sum_{n=0}^{N-1} r_n s_n^* e^{-j2\pi\delta n}}{\sum_{n=0}^{N-1} |s_n|^2}, \tag{9}$$

so that $\hat{\phi} = \arg\{S\}$.

The frequency estimate $\hat{\delta}$ is obtained similarly as the zero of the derivative of (8) and plugging the optimal phasor (9) into the resulting expression,

$$\sum_{n=0}^{N-1} (r_n s_n^* S^* n e^{-j2\pi\hat{\delta}n} - s_n s_n^* n) = 0. \tag{10}$$

Note $\sum_{n=0}^{N-1} s_n s_n^* n$ is real valued, which results the imaginary part of left hand side of (10) be zero; By putting the estimate for S in (10) and rearranging the order of indexes, yields

$$\Im\left\{\sum_{m=0}^{N-1}\sum_{n=0}^{N-1} n r_n r_m^* s_n^* s_m e^{j2\pi\hat{\delta}(m-n)}\right\} = 0. \tag{11}$$

A change of variables lets us focus on the difference between sampling instances m and n. Let $k = m - n$, (11) becomes

$$\Im\left\{\sum_{m=0}^{N-1}\sum_{k=m-(N-1)}^{m} (m-k) r_{m-k} r_m^* s_{m-k}^* s_m e^{j2\pi\hat{\delta}k}\right\} = 0. \tag{12}$$

Reversing the order of summation in (12), we get

$$\Im\left\{\sum_{k=-(N-1)}^{0}\sum_{m=0}^{N-1+k} (m-k) r_{m-k} r_m^* s_{m-k}^* s_m e^{j2\pi\hat{\delta}k} + \sum_{k=1}^{N-1}\sum_{m=k}^{N-1} (m-k) r_{m-k} r_m^* s_{m-k}^* s_m e^{j2\pi\hat{\delta}k}\right\} = 0. \tag{13}$$

It is self-explanatory (13) for $k = 0$ can be eliminated because of real-valued. For $k \neq 0$, the positive and negative index k are symmetry. After grouping terms appropriately, the necessary condition for $\hat{\delta}$ is given by

$$J(\hat{\delta}) = \Im\left\{\sum_{k=1}^{N-1}\sum_{m=k}^{N-1} k r_{m-k} r_m^* s_{m-k}^* s_m e^{j2\pi\hat{\delta}k}\right\} = 0. \tag{14}$$

This expression is fundamentally equivalent to conditions provided by Luise and Reggiannini [6] and Fitz [7]. However, (14) explicitly allows for pulse shaping and oversampling.

The estimator $\hat{\delta}$ in (14) has no closed-form solution. In [6], it is approximated by replacing the exponential with its Taylor series expansion. In [7], an approximate solution is obtained via Euler's identity for large N. Both solutions have computational complexity $O(N^2)$ reflecting the double summation.

We propose a family of alternative solutions to (14). A solution with $O(N)$ complexity is used for operating at the sample rate during the sequential GLRT detection; it prioritizes low complexity at the expense of some loss of accuracy. A second solution is used to improve the estimation accuracy for coherent demodulation once the preamble has been detected.

A. Solution I: Single-Difference (SD) Estimator

The first estimator is rooted in the insight that at high SNR environment, every lag k in (14) can be used to approximate the true frequency offset $\bar{\delta}$. Assume noise is very small, i.e., $r_m \approx s_m A e^{j(2\pi\bar{\delta}m+\phi)}$. (14) can be expanded to

$$\Im\left\{A^2 \sum_{k=1}^{N-1}\sum_{m=k}^{N-1} k|s_{m-k}|^2|s_m|^2 e^{j2\pi(\hat{\delta}-\bar{\delta})k}\right\} = 0. \quad (15)$$

Note that in (15) the inner summation is purely real for every lag k if $\hat{\delta} = \bar{\delta}$. This observation suggests that an unbiased estimate of the frequency offset can be obtained by using only a single lag k from (14). The approach lowers the complexity from $O(N^2)$ to $O(N)$ and permits a closed-form solution for $\hat{\delta}$.

1) Closed-form expression: For one lag k, the SD estimator is given by

$$\hat{\delta}_{\text{SD}}(k) = -\frac{\arg\left\{\sum_{m=k}^{N-1} r_{m-k} r_m^* s_{m-k}^* s_m\right\}}{2\pi k}. \quad (16)$$

2) Choice of lag k: At low (or normal) SNR environment, i.e., noise effect cannot be ignored, the argument of numerator in (16) can be extended to

$$\sum_{m=k}^{N-1} r_{m-k} r_m^* s_{m-k}^* s_m = \sum_{m=k}^{N-1}\Big(A^2|s_{m-k}|^2|s_m|^2 e^{-j2\pi\bar{\delta}k}+$$
$$w_m^* S|s_{m-k}|^2 s_m e^{j2\pi\bar{\delta}(m-k)} + w_{m-k} S^*|s_m|^2 s_{m-k}^* e^{-j2\pi\bar{\delta}m}+$$
$$w_{m-k} w_m^* s_{m-k}^* s_m\Big). \quad (17)$$

To interpret (17), recognize that the first term of right hand side is deterministic and provides the mean of the expression. The last term can be neglected even at moderate SNR since the factors in the product are uncorrelated (as long as $k \neq 0$). The two middle terms yield a zero-mean, complex Gaussian random variable. If we denote the expression in (17) as random variable $W(k)$, then these observations can be summarized as

$$W(k) \sim \mathcal{CN}\left(\left(\frac{N-k}{A^2}\right)\left(\frac{E_s}{M}\right)^2 e^{-j2\pi\bar{\delta}k}, 2\left(\frac{N-k}{A^4}\right)\frac{N_0}{2}\left(\frac{E_s}{M}\right)^3\right). \quad (18)$$

Here $A^2|s_m|^2 \approx E_s/M$ denotes the average energy per sample.

Recall from (16) the estimator $\hat{\delta}_{\text{SD}}(k)$ requires $\arg\{W(k)\}$. The full pdf of $\arg\{W(k)\}$ is derived in the appendix A where it is also shown that a good approximation, valid for moderate SNR, is Gaussian. Specifically

$$\arg\{W(k)\} \sim \mathcal{N}\left(\angle\mu_{W(k)}, \frac{\sigma^2_{W(k)}}{|\mu_{W(k)}|^2}\right). \quad (19)$$

$\mu_{w(k)}$ and $\sigma^2_{W(k)}$ are the mean and variance of $W(k)$ provided in (18). By plugging (18), (19) into (16), the SD estimator is approximately Gaussian distributed at moderate SNR with pdf

$$\hat{\delta}_{\text{SD}}(k) \sim \mathcal{N}\left(\bar{\delta}, \frac{M}{4\pi^2 k^2 (N-k) E_s/N_0}\right). \quad (20)$$

We can see that $\hat{\delta}_{\text{SD}}(k)$ is unbiased. Moreover, the lag k affects the variance of the SD estimator. One best choice is to choose $k = \frac{2}{3}N$ to minimize the variance.

It should be noted that, to prevent "aliasing" of the frequency estimate, it's also required to choose the lag k small enough to ensure $2\pi|\bar{\delta}|k < \pi$. Assuming an upper bound $\delta_{\max}$ on the normalized frequency offset is available, the optimal choosing policy for lag k_{opt} is refined as

$$k_{\text{opt}} = \begin{cases} \lfloor\frac{2}{3}N\rfloor & \text{for } \frac{1}{2\delta_{\max}} > \lfloor\frac{2}{3}N\rfloor \\ \lceil\frac{1}{2\delta_{\max}} - 1\rceil & \text{for } \frac{1}{2\delta_{\max}} \leq \lfloor\frac{2}{3}N\rfloor, \end{cases} \quad (21)$$

where $\lfloor\cdot\rfloor$ and $\lceil\cdot\rceil$ are the floor and ceil operation, respectively.

3) Low-SNR Improvement: Recall the SD estimator is introduced by assuming SNR is relatively high. The accuracy of the SD estimator may also be crucial at low SNR. One way to improving it is by averaging K numbers of SD estimators with different lags k. We call the resulting estimator the K-SD estimator, $\hat{\delta}_{K\text{-SD}}$. In this case, we trade off a K-fold increase in computational complexity for lower variance.

Let $\boldsymbol{u}$ be a vector of non-negative, with $\sum_{k\in\mathcal{K}} u_k = 1$; here $\mathcal{K}$ represents the set of K lags to be averaged. Simple linear combining of K SD estimators yields the K-SD estimator

$$\hat{\delta}_{K\text{-SD}} = \sum_{k\in\mathcal{K}} \hat{\delta}_{\text{SD}}(k) u_k. \quad (22)$$

One optimal weight vector $\boldsymbol{u}_{\text{opt}}$ can be obtained by minimizing the variance of $\hat{\delta}_{K\text{-SD}}$, which is well-known as

$$\boldsymbol{u}_{\text{opt}} = \frac{\boldsymbol{C}^{-1}\mathbf{1}}{\mathbf{1}^T \boldsymbol{C}^{-1}\mathbf{1}}. \quad (23)$$

$\boldsymbol{C}$ is the autocovariance matrix between the K SD estimators and $\mathbf{1}$ represents the column vector of one. Unfortunately, it is generally difficult to know the full information of $\boldsymbol{C}$. However, If the lags $k \in \mathcal{K}$ are chosen to satisfy the spacing between any pair is at least equal to the oversampling factor M, then the estimates to be combined are approximately uncorrelated and unbiased; The resulting $\boldsymbol{C}$ is a diagonal matrix of variance of each SD estimator. For example, a good choice for selecting 3 lags is $\mathcal{K} = \{k_{\text{opt}} - M, k_{\text{opt}}, k_{\text{opt}} + M\}$. The optimal weights $\boldsymbol{u}_{\text{opt}}$ are proportional to the inverse of the variances in (20).

B. Solution II: Newton-Method (NM) Estimator

The SD estimator emphasizes low-complexity property and is intended to provide merely sufficiently good carrier synchronization to enable coherent detection. Once the signal has been acquired, the SD estimator can be improved by investing additional computations. Since detection events are rare, the computational complexity is of little concern.

The principle is to use the SD (or K-SD) estimator as the starting point for a Newton-type iteration aimed at finding a better solution to the necessary condition (14). In principle, multiple iterations are possible to produce successively better approximations to the root of $J(\hat{\delta})$ in (14). Specifically, the iterations are given by
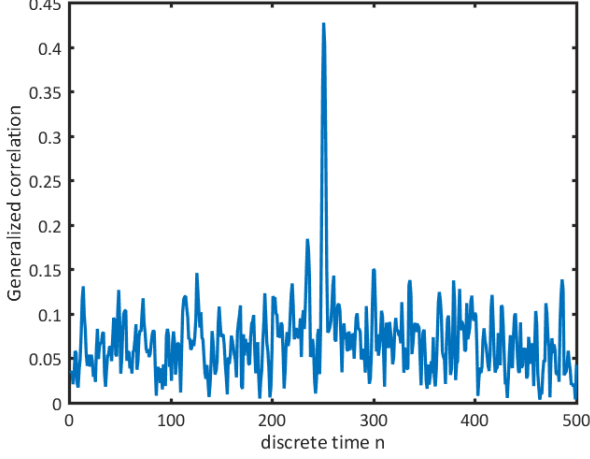
Fig. 2. Performance of GLRT based detector of (7) via the received stream

Fig. 3. Receiver operating characteristics of detector for different SNR

$$\hat{\delta}_{NM}^{(i+1)} = \hat{\delta}_{NM}^{(i)} - \frac{J(\hat{\delta}_{NM}^{(i)})}{J'(\hat{\delta}_{NM}^{(i)})} \qquad (24)$$

where $\hat{\delta}_{NM}^{(0)} = \hat{\delta}_{SD}(k_{opt})$ is the starting point of the iteration and $J'(\cdot)$ denotes the derivative of J with respect to $\hat{\delta}$. Specifically,

$$J'(\hat{\delta}) = \Im\left\{ \sum_{k=1}^{N-1} \sum_{m=k}^{N-1} j2\pi k^2 r_{m-k} r_m^* s_{m-k}^* s_m e^{j2\pi\hat{\delta}k} \right\}. \qquad (25)$$

Our simulations indicate that only a single iteration is usually sufficient to achieve very good accuracy.

V. SIMULATION RESULTS

The simulation section illustrates the results in the order of detection, estimation and joint detection and estimation. Four different lengths of reference symbol sequences are simulated with 50% rolloff Square-Root Raised Cosine (SRRC) pulses. The reference symbols are chosen randomly from a QPSK alphabet with good autocorrelation properties. We assume the normalized frequency offset is small enough so that the design parameter k of the SD estimator can be chosen optimally by 2/3 length of the preamble, i.e., top of (21).

A. Simulation Results for Detection

Figure 2 illustrates the performance of the proposed detector of (7). We see from the figure that it does not show a perfect autocorrelation property after pulse shaping, e.g., around the position of the preamble, the correlation decays very slow. The problem happens that it makes (7) much more challengable to choose the threshold to distinguish between the real position of the preamble and its corresponding adjacent positions. The solution to mitigating it is to adjust the detection algorithm by changing making the decisions at each observation individually (by comparing the correlation and threshold) to finding the local maximum of the correlation.
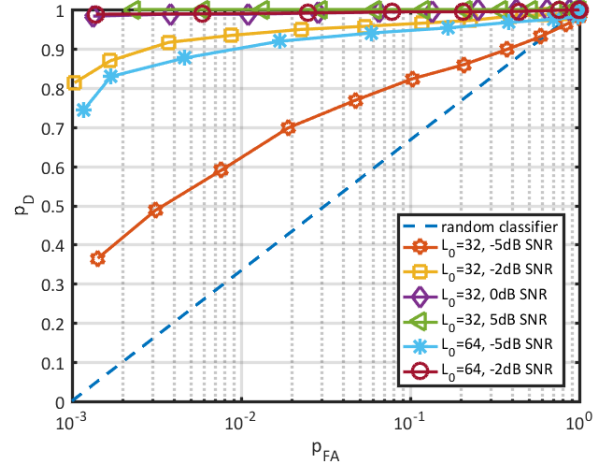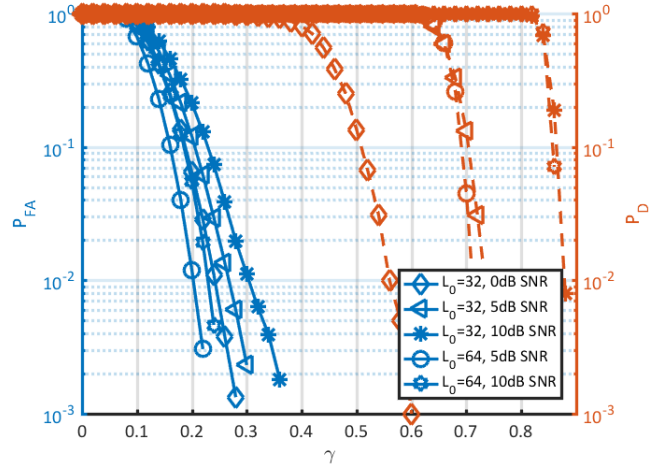

Fig. 4. False alarm and detection ratio for different SNR and size of preamble

Figure 3 shows the receiver operating characteristics (ROC) of the proposed (adjusted) detector. It basically illustrates that the detector has good ROCs at moderate SNR. Specifically, the detector achieves perfect ROCs for positive SNR (in decibel); Moreover, it is robust to low SNR environment, e.g., we can pick such a threshold to achieve 10^{-3} false alarm probability and 0.75 detection probability simultaneously. However, it is not clear from this figure to pick an exact threshold for certain detection purpose.

Figure 4 shows the performance of detector but from another perspective. Specifically, it gives us a clearer insight into the false alarm and detection probabilities via the threshold. It is common that it's hard to pick such a threshold to accommodate all specific detection purposes. For simulation purpose, if we want to determine a threshold to work for the reference signal sequence with $L_0 \geq 32$ and up to 10 dB SNR, Based on Figure 4 and Neyman-Pearson criterion, $\gamma = 0.43$ is a good choice to meet $P_{FA} < 1e^{-3}$ and nearly perfect P_D.
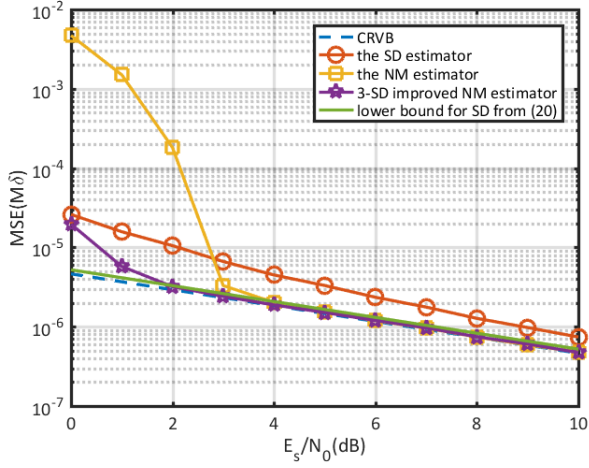
Fig. 5. Accuracy of the SD and SD (or K-SD) based NM estimators ($L_0 = 32$)
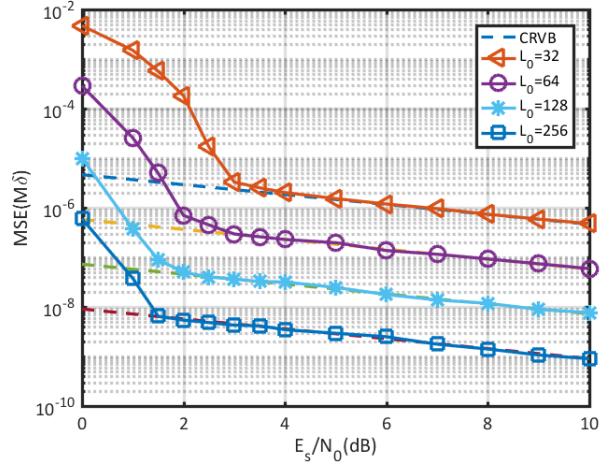

Fig. 7. Accuracy of NM frequency estimate in joint detection and estimation ($\gamma = 0.43$)
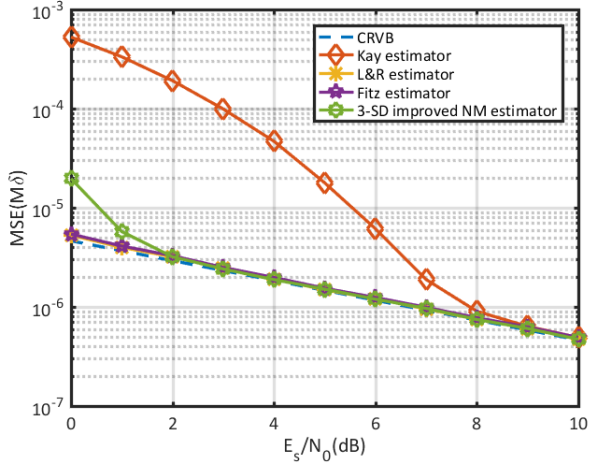

Fig. 6. Accuracy of the NM and traditional estimators ($L_0 = 32$)

Fig. 8. Accuracy of the NM phase estimate in joint detection and estimation ($\gamma = 0.43$)

B. Simulation Results for Estimation

For simulation purpose, we assume that the detection progress is perfect in this section. Figure 5 emphasizes illustrating the accuracy of the two proposed estimators, the SD estimator of (16) and the NM estimator of (24) in this paper. The lower dashed line denotes the Cramer-Rao vector bound (CRVB) for frequency estimate, which is given by

$$\text{CRVB}(M\delta) \geq \frac{3}{2\pi^2 L_0^3 E_s/N_0}. \qquad (26)$$

Furthermore, the CRVB for ϕ is derived as

$$\text{CRVB}(\phi) \geq \frac{2}{L_0 E_s/N_0}. \qquad (27)$$

The derivations of (26) and (27) are given in Appendix B.

In Figure 5, we see the NM estimator approaches the CRVB. The accuracy of the SD estimator is crucial not only just for building the GLRT detector but deciding the accuracy of the
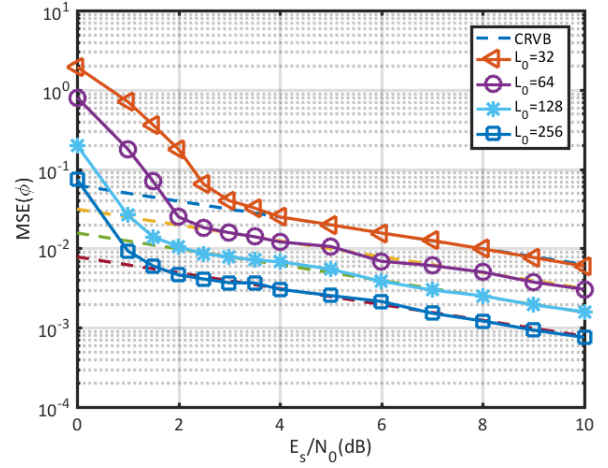
NM estimator. The evidence is that the NM estimator performs even worse than the SD estimator at low SNR. This is because the Newton iteration of (24) converges occasionally to local minimum away from the true frequency offset if the beginning estimate is really far from. Figure 5 also shows the averaging method of (22) improves the accuracy of the SD estimator thus improves the NM estimator at low SNR.

Figure 6 compares the performance of the NM and traditional estimators in [5]–[7]. Related to Figure 5, we conclude that the NM estimator can achieve as good accuracy as those autocorrelation-based estimators (L&R estimator [6] and Fitz estimator [7]) when the SD estimator is accurate enough. To put it another way, without increasing complexity by averaging with multiple SD estimators, the NM estimator can achieve the same good accuracy as the traditional estimators at moderate SNR.
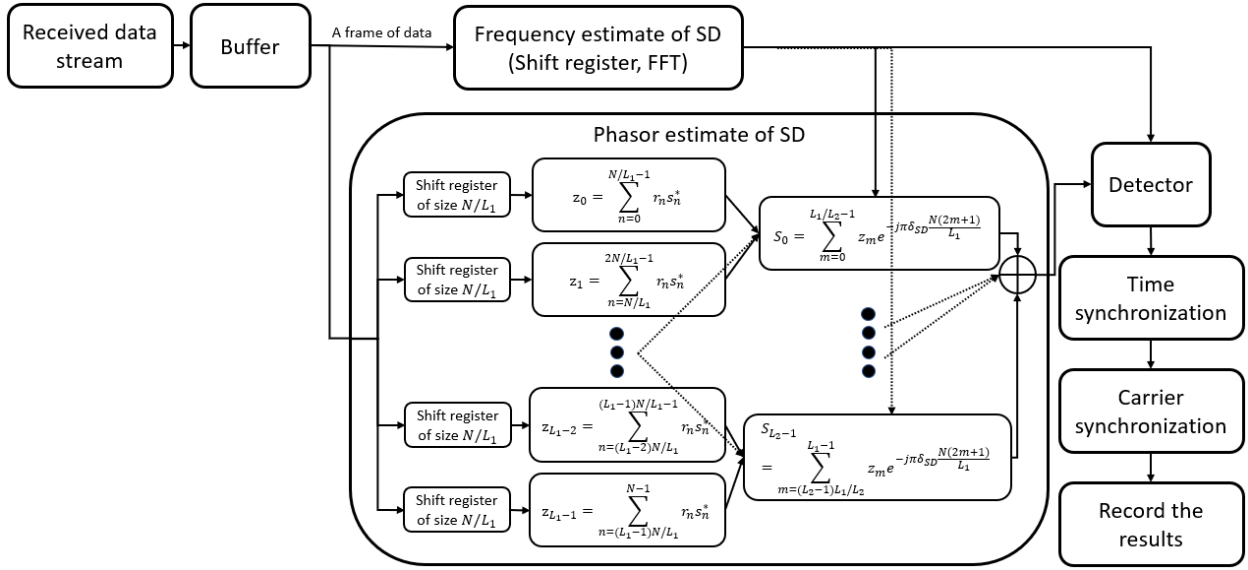
Fig. 9. Block diagram for implementing the proposed algorithm on software-defined radio (some steps are omitted)

C. Simulation Results for Detection and Synchronization

This section simulates the complete signal acquisition chain and shows the simulation results of the last step in Figure 1. Figure 7 and 8 illustrate the performance of our proposed joint detection and carrier synchronization algorithm. No averaged SD estimator is used because we want to reduce the complexity of the sequential detection process. Compared with Figure 4 and Figure 5, the reason for the NM estimator not approaching the CRVB at low SNR is due to the non-sufficient accuracy of the SD estimator. Besides that, we can also get a common result that by increasing the size of the preamble, better performance of carrier synchronization is realized and CRVB is approached at lower SNR.

VI. IMPLEMENTATION ON SOFTWARE-DEFINED RADIO

Two main aspects of measuring the performance of modern communcation systems, except for accuracy, are the latency and throughput. In the previous sections, we focus on explaining and showing how much accuracy of our proposed joint detection and estimation algorithm can be. In order to realize it on software-defined radio (SDR), the algorithm, especially the detection algorithm, should be refined to fitting very high sample rate since it is applied on every time instant.

A. Receiver Side (algorithm)

Figure 9 illustrates some detailed changes of our proposed algorithm. First, the style of the observation window with feedback loop in Figure 1 is eliminated because it incurs a very large amount of overhead. Instead, the received data is directly buffered into a fixed size (normally larger than the length of the preamble) of frame without overlapping. Now the problem may happen when the preamble in the received data is cut off over two frames. The shift register is reused after the buffer to solve this problem. Compared with the old

method, the received data packed in frames can be processed in order without waiting for the result of detecting; Moreover, the length of the shift register can be also reduced. For example, if we look at formula of the SD estimator in (16), the length of the shift register can be shortened from N to $k + 1$, i.e., if $k = \frac{2}{3}N$, the overhead is approximately reduced by $\frac{N}{3}$.

Second, some key steps of the proposed detection algorithm should be computed more efficiently. For example, to calculate the frequency estimate of SD estimator, (16) can be intepreted as the convolution between autocorrelation vector of received samples and of the preamble (one of them should be reversed). Thus, the most efficient way of calculating (16) could be the fast fourier transform (FFT).

Another important improvement that should be emphasized is about calculating the phase (phasor) estimate of the SD estimator in (9). No te, (9) is a time-varying convolution, which cannot be computed by FFT. To approximate the dot product in (9), we re-order the computation by first calculating the dot product between the (partial) received data vector (r) and the (partial) preamble (s); the result is then corrected (multiplied) by the frequency estimate at the middle position of data vector and added together. Specifically, the numerator of

$$\hat{S} \approx \sum_{i=0}^{L_2-1} \sum_{m=iL_1/L_2}^{(i+1)L_1/L_2-1} \sum_{n=mN/L_1}^{(m+1)N/L_1-1} r_n s_n^* e^{-j\pi\hat{\delta}\frac{N(2m+1)}{L_1}}. \quad (28)$$

As illustrated in Figure 9, we compute (28) in two stages, each stage contains L_1 (or L_2) parallel sub cells. Thus, we achieve the functional parallelism by an approximate of $L_1 \cdot L_2$ speed up. To get a good approximation, L_1 should not be too small and L_2 is the factor of L_1.

B. Signal Transmission Path

In this section, we briefly talk about the signal transmitting path, which is used for testing our algorithm. The hardware connection is fairly easy. Each of two processors (computers) connected to a universal software radio peripheral (USRP) by one 5-Gigabit Ethernet cable as the transmitter or receiver. Between two USRPs, a cable with 30 dB attenuation connects the RX/TX port and RX port. At the transmitter side, the processor needs to tell the (transmitter) USRP the sample rate, the baseband signal and frequency, the carrier frequency, the transmitter gain, etc. Then, the USRP transmits the analog signal to the (receiver) USRP through the two ports. At the receiver side, the received analog RF signal is first down-converted to baseband, down-sampled to discrete-time data stream and finally stored in the local network. After that, our proposed algorithm as illustrated in Figure 9 can be tested by requesting the data from the local network.

C. Performance of SDR

To measure the performance of the SDR, we focus on the accuracy, throughput and latency of our proposed algorithm. Some parameters in Figure 9 should be chosen by the following rules: First, the length of the preamble should be chosen short enough to get the largest throughput as long as it does not degrade the accuracy; Second, the length of frame should be chosen as the power of 2 to achieve the best performance of FFT; Moreover, it trades off between the overhead and latency, e.g., short frame has small latency but large overhead. Third, as discussed above, L_1 in (28) should not be chosen too small for a good approximation of phasor estimate. However, the large number of parallel executions will occupy the most threads of the computer.

As tested, such parameters are determined that can achieve a relatively good performance: The preamble is chosen with the number of symbols $L_0 = 32$ and oversampling factor $M = 4$. the length of the frame is determined by 8192; Four complete preambles are embedded in each frame. The number of sub cells for two stages are $L_1 = 2L_2 = 16$. Furthermore, some parameters of USRP are set as follows: The sample rate at transmitter is 10 MS/s; The transmitter gain plus receiver gain is 20 dB. Based on above, we get the maximum throughput is around 4.5 MS/s and the latency is near 1 ms; The detection algorithm is very robust and the false alarm probability is near 0.

APPENDIX A
DERIVATION OF DISTRIBUTION FOR THE SD ESTIMATOR, PROOF OF (19)

To prove the distribution of $\arg\{W(k)\}$, where $W(k)$ is a complex Gaussian random variable, we assume $W = X + jY$, X and Y are two Gaussian random variables with distributions $X \sim \mathcal{N}(\mu_x, \sigma^2)$ and $Y \sim \mathcal{N}(\mu_y, \sigma^2)$. Here, W, X, Y, μ_x, μ_y and σ^2 all depends on k, we just write those for notation simplicity. We further assume μ_w to be the mean of W. The probability density function of W is given by

$$
\begin{aligned}
&f_W(w) \\
&= f_{X,Y}(x, y) = \frac{1}{2\pi\sigma^2} \exp\left(-\frac{(x - \mu_x)^2 + (y - \mu_y)^2}{2\sigma^2}\right).
\end{aligned} \tag{29}
$$

Let $x = r\cos\theta$, $y = r\sin\theta$, (29) can be transformed into polar coordinate,

$$
\begin{aligned}
&f_W(w) = f_{R,\Theta}(r, \theta) \\
&= \frac{r}{2\pi\sigma^2} \exp\left(-\frac{(r\cos\theta - \mu_x)^2 + (r\sin\theta - \mu_y)^2}{2\sigma^2}\right) \\
&= \frac{r}{2\pi\sigma^2} \exp\left(-\frac{r^2 + \mu_x^2 + \mu_y^2}{2\sigma^2}\right) \exp\left(\frac{r}{\sigma^2}(\mu_x\cos\theta + \mu_y\sin\theta)\right)
\end{aligned} \tag{30}
$$

Plugging $\mu_x = |\mu_w|\cos(\angle\mu_w)$, $\mu_y = |\mu_w|\sin(\angle\mu_w)$ yields

$$
\begin{aligned}
&f_{R,\Theta}(r, \theta) \\
&= \frac{r}{2\pi\sigma^2} \exp\left(-\frac{r^2 + |\mu_w|^2}{2\sigma^2}\right) \exp\left(\frac{r|\mu_w|}{\sigma^2}\cos(\theta - \angle\mu_w)\right).
\end{aligned} \tag{31}
$$

Note that $\theta = \arg\{W(k)\}$. Thus, we turn our attention to marginal PDF of θ,

$$
\begin{aligned}
f_\Theta(\theta) &= \int_0^\infty \frac{r}{2\pi\sigma^2} \exp\left(-\frac{r^2 - 2r|\mu_w|\cos(\theta - \angle\mu_w) + |\mu_w|^2}{2\sigma^2}\right) dr \\
&= \int_0^\infty \frac{r}{2\pi\sigma^2} \cdot \\
&\exp\left(-\frac{(r - |\mu_w|\cos(\theta - \angle\mu_w))^2 + |\mu_w|^2(1 - \cos^2(\theta - \angle\mu_w))}{2\sigma^2}\right) dr \\
&= \frac{1}{2\pi} \exp\left(-\frac{|\mu_w|^2(1 - \cos^2(\theta - \angle\mu_w))}{2\sigma^2}\right) \cdot \\
&\int_0^\infty \frac{r}{\sigma^2} \exp\left(-\frac{(r - |\mu_w|\cos(\theta - \angle\mu_w))^2}{2\sigma^2}\right) dr.
\end{aligned} \tag{32}
$$

By assuming

$$
\begin{aligned}
\alpha &= |\mu_w|\sin(\theta - \angle\mu_w) \\
\beta &= |\mu_w|\cos(\theta - \angle\mu_w) \\
u &= \frac{r - |\mu_w|\cos(\theta - \angle\mu_w)}{\sigma},
\end{aligned}
$$

(32) can be simplified as

$$f_\Theta(\theta)=\frac{1}{2\pi}\exp\left(-\frac{\alpha^2}{2\sigma^2}\right)\int_{-\frac{\beta}{\alpha}}^{\infty}\left(u+\frac{\beta}{\alpha}\right)\exp\left(-\frac{u^2}{2}\right)du$$

$$=\frac{1}{2\pi}\exp\left(-\frac{\alpha^2}{2\sigma^2}\right)\left(\int_{-\frac{\beta}{\alpha}}^{\infty}ue^{-\frac{u^2}{2}}du+\int_{-\frac{\beta}{\alpha}}^{\infty}\frac{\beta}{\alpha}e^{-\frac{u^2}{2}}du\right)$$

$$=\frac{1}{2\pi}\exp\left(-\frac{\alpha^2+\beta^2}{2\sigma^2}\right)+\frac{\beta}{\sqrt{2\pi}\sigma}\exp\left(-\frac{\alpha^2}{2\sigma^2}\right)Q\left(-\frac{\beta}{\alpha}\right)$$

$$=\frac{1}{2\pi}\exp\left(-\frac{|\mu_w|^2}{2\sigma^2}\right)+\frac{|\mu_w|\cos(\theta-\angle\mu_w)}{\sqrt{2\pi}\sigma}\cdot$$
$$\exp\left(-\frac{|\mu_w|^2\sin^2(\theta-\angle\mu_w)}{2\sigma^2}\right)Q\left(-\frac{|\mu_w|}{\sigma}\cos(\theta-\angle\mu_w)\right) \tag{33}$$

where $Q(\cdot)$ is the Q function and (33) gives the explicit marginal PDF for θ. Note that $|\mu_w|=(N-k)(\frac{E_s}{T})^2$ from (18). Thus, at relatively high SNR, i.e., $|\mu_w|\gg\sigma$, (33) can be approximated by

$$f_\Theta(\theta)\approx\frac{1}{2\pi}\exp\left(-\frac{|\mu_w|^2}{2\sigma^2}\right)$$
$$+\frac{|\mu_w|\cos(\theta-\angle\mu_w)}{\sqrt{2\pi}\sigma}\exp\left(-\frac{|\mu_w|^2\sin^2(\theta-\angle\mu_w)}{2\sigma^2}\right)\cdot$$
$$\left(1-\frac{\sigma}{\sqrt{2\pi}|\mu_w|\cos(\theta-\angle\mu_w)}\exp\left(-\frac{|\mu_w|^2\cos^2(\theta-\angle\mu_w)}{2\sigma^2}\right)\right)$$
$$=\frac{|\mu_w|\cos(\theta-\angle\mu_w)}{\sqrt{2\pi}\sigma}\exp\left(-\frac{|\mu_w|^2\sin^2(\theta-\angle\mu_w)}{2\sigma^2}\right) \tag{34}$$

The approximation holds because of the property of Q function $Q(x)\approx\frac{1}{\sqrt{2\pi}x}\exp\left(-\frac{x^2}{2}\right)$ for $x\gg0$. Then, we only need to look at $f_\Theta(\theta)$ where $\theta\approx\angle\mu_w$, i.e.,

$$f_\Theta(\theta)\approx\frac{|\mu_w|}{\sqrt{2\pi}\sigma}\exp\left(-\frac{|\mu_w|^2}{2\sigma^2}(\theta-\angle\mu_w)^2\right) \tag{35}$$

Thus, θ is approximately Gaussian with the distribution $\theta\sim\mathcal{N}\left(\angle\mu_W,\frac{\sigma^2}{|\mu_w|^2}\right)$, which is equivalent to (19).

APPENDIX B
DERIVATION OF THE CRVB FOR FREQUENCY AND PHASE ESTIMATE, PROOF OF (26) AND (27)

In order to derive the CRVB for joint estimation of phase and frequency offset, We define a parameter vector $\boldsymbol{\theta}\triangleq\begin{bmatrix}\delta & \phi\end{bmatrix}$ to include the two parameters that we want to estimate. The first step towards the derivation of the CRVB is to compute the Fisher Information Matrix (FIM, $\boldsymbol{I}(\boldsymbol{\theta})$). The calculation of $\boldsymbol{I}(\boldsymbol{\theta})$ is based on log-likelihood function ($\ln\Lambda$), which is carried out in [18, Ch. 4]

$$\ln\Lambda[r(t),\boldsymbol{\theta}]=\frac{2}{N_0}\int_0^{T_0}r(t)s'^*(t,\boldsymbol{\theta})dt-\frac{1}{N_0}\int_0^{T_0}|s'(t,\boldsymbol{\theta})|^2dt \tag{36}$$

where

$$s'(t,\boldsymbol{\theta})=Ae^{j(2\pi\delta t+\phi)}\sum_{i=0}^{L_0-1}c_ig(t-iT), \tag{37}$$

and T_0 is the observation length. Taking the second derivative with respect to each element of the parameter vector θ_i, θ_j yields

$$\frac{\partial^2\ln\Lambda}{\partial\theta_i\partial\theta_j}$$
$$=\frac{2}{N_0}\int_0^{T_0}r(t)\frac{\partial^2s'^*(t,\boldsymbol{\theta})}{\partial\theta_i\partial\theta_j}dt-\frac{2}{N_0}\int_0^{T_0}\frac{\partial s'^*(t,\boldsymbol{\theta})}{\partial\theta_i}\frac{\partial s'(t,\boldsymbol{\theta})}{\partial\theta_j}dt$$
$$-\frac{2}{N_0}\int_0^{T_0}s'(t,\boldsymbol{\theta})\frac{\partial^2s'^*(t,\boldsymbol{\theta})}{\partial\theta_i\partial\theta_j}dt. \tag{38}$$

Taking the negative expectation of (38), the elements of FIM are given by

$$\boldsymbol{I}(\boldsymbol{\theta})_{ij}=-\mathbb{E}\left[\frac{\partial^2\ln\Lambda}{\partial\theta_i\partial\theta_j}\right]=\frac{2}{N_0}\int_0^{T_0}\frac{\partial s'^*(t,\boldsymbol{\theta})}{\partial\theta_i}\frac{\partial s'(t,\boldsymbol{\theta})}{\partial\theta_j}dt. \tag{39}$$

By plugging $s'(t,\boldsymbol{\theta})$ from (37) into (39) and replacing θ_i, θ_j with δ,δ, the first element of FIM ($\boldsymbol{I}(\boldsymbol{\theta})_{11}$) yields

$$\boldsymbol{I}(\boldsymbol{\theta})_{11}=\frac{2}{N_0}\int_0^{T_0}\frac{\partial Ae^{j(2\pi\delta t+\phi)}\sum_{i=0}^{L_0-1}c_ig(t-iT)}{\partial\delta}\cdot$$
$$\frac{\partial Ae^{-j(2\pi\delta t+\phi)}\sum_{i=0}^{L_0-1}c_i^*g^*(t-iT)}{\partial\delta}dt \tag{40}$$
$$=\frac{2}{N_0}\int_0^{T_0}A^24\pi^2t^2\left|\sum_{i=0}^{L_0-1}c_ig(t-iT)\right|^2dt.$$

Note that the averaged symbol energy of transmitted signal is calculated by

$$E_s=\int_0^T\left|A\sum_{i=0}^{L_0-1}c_ig(t-iT)\right|^2dt$$
$$\approx\sum_{k=0}^{M-1}\left|A\sum_{i=0}^{L_0-1}c_ig(kT_s-iT)\right|^2T_s \tag{41}$$
$$\approx T\left|A\sum_{i=0}^{L_0-1}c_ig(t-iT)\right|^2,$$

or,

$$A^2\left|\sum_{i=0}^{L_0-1}c_ig(t-iT)\right|^2\approx\frac{E_s}{T}. \tag{42}$$

where $M=\text{int}(T/T_s)$. The first approximation in (41) is based on Riemann sum theory. $\boldsymbol{I}(\boldsymbol{\theta})_{11}$ finally results in

$$\boldsymbol{I}(\boldsymbol{\theta})_{11}=\frac{8\pi E_sT_0^2L_0}{3N_0}. \tag{43}$$

Similarly, $I(\boldsymbol{\theta})_{12}$ can be calculated by plugging $s'(t,\boldsymbol{\theta})$ from (37) into (39) and replacing θ_i, θ_j with δ, ϕ, which is given by

$$I(\boldsymbol{\theta})_{12} = \frac{2}{N_0} \int_0^{T_0} \frac{\partial A e^{j(2\pi\delta t + \phi)} \sum_{i=0}^{L_0-1} c_i g(t-iT)}{\partial \delta} \cdot$$
$$\frac{\partial A e^{-j(2\pi\delta t + \phi)} \sum_{i=0}^{L_0-1} c_i^* g^*(t-iT)}{\partial \phi} dt. \tag{44}$$

Following the same steps as deriving $I(\boldsymbol{\theta})_{11}$, $I(\boldsymbol{\theta})_{12}$ can be finally reduced to

$$I(\boldsymbol{\theta})_{12} = \frac{2\pi E_s T_0 L_0}{N_0}. \tag{45}$$

$I(\boldsymbol{\theta})_{22}$ can be calculated by plugging $s'(t,\boldsymbol{\theta})$ from (37) into (39) and replacing θ_i, θ_j with ϕ, ϕ, which is given by

$$I(\boldsymbol{\theta})_{22} = \frac{2}{N_0} \int_0^{T_0} \frac{\partial A e^{j(2\pi\delta t + \phi)} \sum_{i=0}^{L_0-1} c_i g(t-iT)}{\partial \phi} \cdot$$
$$\frac{\partial A e^{-j(2\pi\delta t + \phi)} \sum_{i=0}^{L_0-1} c_i^* g^*(t-iT)}{\partial \phi} dt. \tag{46}$$

$I(\boldsymbol{\theta})_{22}$ can be finally reduced to

$$I(\boldsymbol{\theta})_{22} = \frac{2E_s L_0}{N_0}. \tag{47}$$

Then, $I(\boldsymbol{\theta})_{11}$, $I(\boldsymbol{\theta})_{12}$ and $I(\boldsymbol{\theta})_{22}$ form the FIM

$$I(\boldsymbol{\theta}) = \begin{bmatrix} \frac{8\pi E_s T_0^2 L_0}{3 N_0} & \frac{2\pi E_s T_0 L_0}{N_0} \\ \frac{2\pi E_s T_0 L_0}{N_0} & \frac{2E_s L_0}{N_0} \end{bmatrix}, \tag{48}$$

and the inverse FIM is given by

$$I^{-1}(\boldsymbol{\theta}) = \begin{bmatrix} \frac{3}{2\pi^2 L_0 T_0^2 E_s / N_0} & \frac{-3}{2\pi L_0 T_0 E_s / N_0} \\ \frac{-3}{2\pi L_0 T_0 E_s / N_0} & \frac{2}{L_0 E_s / N_0} \end{bmatrix}. \tag{49}$$

Thus, the CRVB for the frequency and phase estimates are

$$\mathrm{CRVB}(\delta) \geq \frac{3}{2\pi^2 L_0 T_0^2 E_s / N_0}$$
$$\mathrm{CRVB}(\phi) \geq \frac{2}{L_0 E_s / N_0}, \tag{50}$$

which are equivalent to (26) and (27) respectively by replacing T_0 with N.

References

[1] D. D. Falconer, F. Adachi, and B. Gudmundson, "Time division multiple access methods for wireless personal communications," *IEEE Communications Magazine*, vol. 33, no. 1, pp. 50–57, 1995.

[2] M. Morelli and U. Mengali, "Feedforward frequency estimation for PSK: A tutorial review," *European Transactions on Telecommunications*, vol. 9, pp. 103–116, 1998.

[3] D. Rife and R. Boorstyn, "Single tone parameter estimation from discrete-time observations," *IEEE Transactions on Information Theory*, vol. 20, no. 5, pp. 591–598, 1974.

[4] S. Tretter, "Estimating the frequency of a noisy sinusoid by linear regression (corresp.)," *IEEE Transactions on Information Theory*, vol. 31, no. 6, pp. 832–835, 1985.

[5] S. Kay, "A fast and accurate single frequency estimator," *IEEE Transactions on Acoustics, Speech, and Signal Processing*, vol. 37, no. 12, pp. 1987–1990, 1989.

[6] M. Luise and R. Reggiannini, "Carrier frequency recovery in all-digital modems for burst-mode transmissions," *IEEE Transactions on Communications*, vol. 43, no. 2/3/4, pp. 1169–1178, 1995.

[7] M. P. Fitz, "Further results in the fast estimation of a single frequency," *IEEE Transactions on Communications*, vol. 42, no. 234, pp. 862–864, 1994.

[8] U. Mengali and M. Morelli, "Data-aided frequency estimation for burst digital transmission," *IEEE Transactions on Communications*, vol. 45, no. 1, pp. 23–25, 1997.

[9] P. Kumari, N. Gonzalez-Prelcic, and R. W. Heath, "Investigating the IEEE 802.11ad standard for millimeter wave automotive radar," in *2015 IEEE 82nd Vehicular Technology Conference (VTC2015-Fall)*, pp. 1–5, 2015.

[10] W. Liu, T. Wei, Y. Huang, C. Chan, and S. Jou, "All-digital synchronization for SC/OFDM mode of IEEE 802.15.3c and IEEE 802.11ad," *IEEE Transactions on Circuits and Systems I: Regular Papers*, vol. 62, no. 2, pp. 545–553, 2015.

[11] E. Grossi, M. Lops, L. Venturino, and A. Zappone, "Opportunistic radar in IEEE 802.11ad networks," *IEEE Transactions on Signal Processing*, vol. 66, no. 9, pp. 2441–2454, 2018.

[12] S. K. Bolisetti, K. Ahmed, M. Patwary, and M. Abdel-Maguid, "Compressive parametric GLRT detector for airborne MIMO radar," in *2011 International Conference on Wireless Communications and Signal Processing (WCSP)*, pp. 1–5, 2011.

[13] Guolong Cui, Lingjiang Kong, Xiaobo Yang, and Jianyu Yang, "Coincidence of the rao test, wald test, and GLRT of MIMO radar in gaussian clutter," in *2009 IET International Radar Conference*, pp. 1–4, 2009.

[14] A. Kumar, S. Dwivedi, and A. K. Jagannatham, "GLRT-based spectrum sensing for MIMO SC-FDMA cognitive radio systems in the presence of synchronization impairments," *IEEE Wireless Communications Letters*, vol. 5, no. 3, pp. 280–283, 2016.

[15] J. Massey, "Optimum frame synchronization," *IEEE Transactions on Communications*, vol. 20, no. 2, pp. 115–119, 1972.

[16] Gee Lui and H. Tan, "Frame synchronization for direct-detection optical communication systems," *IEEE Transactions on Communications*, vol. 34, no. 3, pp. 227–237, 1986.

[17] R. Scholtz, "Frame synchronization techniques," *IEEE Transactions on Communications*, vol. 28, no. 8, pp. 1204–1213, 1980.

[18] H. L. Van Trees, *Detection, estimation, and modulation theory*. New York: Wiley, 1968.